



## Observing Quantum Oscillation of Ground States in Single Molecular Magnet

Jiahui Yang, Ya Wang, Zixiang Wang, Xing Rong, Chang-Kui Duan, Ji-Hu Su,\* and Jiangfeng Du†

*Hefei National Laboratory for Physical Sciences at Microscale and Department of Modern Physics,  
University of Science and Technology of China, Hefei, Anhui 230026, People's Republic of China*

(Received 23 March 2012; published 4 June 2012)

Single molecular magnets (SMMs) are among the potential systems for quantum memory and quantum information processing. Quantum coherence and oscillation are critical for these applications. The ground-state quantum coherence and Rabi oscillations of the SMM  $V_{15}$  ( $[V_{15}^{IV}As_6^{III}O_{42}(H_2O)]^{6-}$ ) have been studied in this context. We have affirmatively measured at 2.4 K the Rabi quantum oscillations and coherence time  $T_2$  for the ground states of the  $V_{15}$  ion of collective spin  $S = 1/2$ , in addition to confirming the previously reported results for the  $S = 3/2$  excited states. The oscillations of  $S = 3/2$  and  $S = 1/2$  states are of different frequencies, and so can be separately selected for purposive manipulations.  $T_2$  of  $188 \pm 4$  ns ( $S = 3/2$ ) and  $149 \pm 10$  ns ( $S = 1/2$ ) are much less than  $T_1 \sim 12$   $\mu$ s and are further extendible via various approaches for qubit implementations.

DOI: 10.1103/PhysRevLett.108.230501

PACS numbers: 03.67.Lx, 03.65.Yz, 03.67.Pp, 76.30.Mi

Single molecular magnet (SMM) refers to the class of molecules with nonzero collective spin showing magnetic property similar to a bulk magnet [1,2]. Since the proposal of quantum computing in SMMs in 2001 [3], quantum oscillations and coherence of SMMs have been subjected to considerable studies [4–10] for the purpose of quantum memory [11] and quantum information processing [12]. Most of the studies have focused on SMMs with large collective spins. In comparison, SMMs with small ground-state spins, such as  $V_{15}$  ( $[V_{15}^{IV}As_6^{III}O_{42}(H_2O)]^{6-}$ ) [13] and  $Cr_7Ni$  [14] have the advantage of substantial smaller coupling with each other and the environment [15] and are likely to be more suitable than SMMs with large collective spins for quantum information applications. Although extensive studies have been carried out on  $V_{15}$  [8,13,16,17], the quantum coherence and Rabi oscillation for the ground spin states ( $S = 1/2$ ), which are critical for quantum information applications, have not been affirmatively observed [8,18]. The claimed first experimental observation in 2008 [8] was unable to be reproduced [18] and turned out to be the signal of cavity background.

In this Letter we report our experimental observations of the ground-state quantum coherence and Rabi oscillation of  $V_{15}$  at a lower temperature of 2.4 K together with scrutinized validation. The results show the possibility of qubit implementation in the ground states of  $V_{15}$ , subject to further lowering the temperature and/or applying various dynamic decoupling approaches to extend the quantum coherent time [19,20].

The  $K_6[V_{15}^{IV}As_6^{III}O_{42}(H_2O)]$  single crystals were prepared as described [13]. Dark brown crystals were collected after three days. One of the crystals was examined by x-ray diffraction (XRD) at room temperature, and the resultant molecular structure is shown in Fig. 1(a) (the K atoms are not depicted). It clearly shows the quasispherical

structure with three layers of vanadium atoms, where two nonplanar hexagons (top and bottom) are separated by the central triangle. This agrees with the reported structure of the  $K_6[V_{15}^{IV}As_6^{III}O_{42}(H_2O)]$  single crystal [13]. The molecule shows a three-fold axis of symmetry ( $C_3$ ) and the core

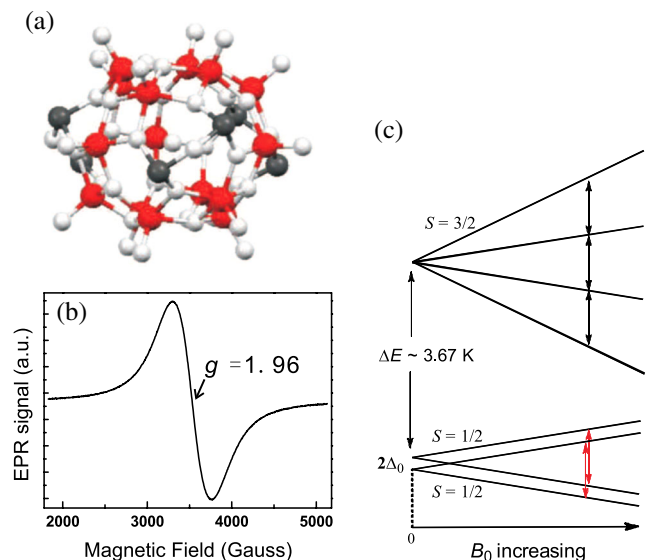


FIG. 1 (color online). (a) Ball-and-stick diagram of molecular structure of  $V_{15}$  gaining from the result of single crystal XRD at room temperature (red, V; black, As; silver, O). (b) Cw spectrum of  $V_{15}$  single crystal at 100 K. Experimental settings: microwave frequency, 9.7 GHz; microwave power, 0.002 mW; modulation frequency, 100 kHz. (c) The energy diagram of  $V_{15}$  low-lying states with the magnetic field parallel to the  $C_3$  axis [8]. The two lower red arrows denote the transitions in the ground doublet states and the three upper black arrows denote those in the first excited states. The energy gap between the excited states and the ground states is about 3.67 K (see text).

is composed of 21 metal ions (15 V and 6 As) ligated by the  $\mu_3$ -oxo-bridges.

The peculiar properties of  $V_{15}$  attracted lots of attention, and the geometric and magnetic/electronic structures of the  $V_{15}$  ion have been studied [13,16] and are summarized: the six spins of the top nonplanar hexagon interact strongly via antiferromagnetic coupling, and the same for the spins of the bottom hexagon. The three spins of the triangle in the middle couple with each other indirectly through superexchange interactions bridged by the nearby spins in the top and bottom hexagons.

Based on the geometrical and electronic structures of  $V_{15}$ , the energy spectrum calculations have shown that the low-lying ground states and the first excited states are isolated from other higher excited states by an energy of around 200 K [8]. Within the set of low-lying states, the energy gap between the ground states ( $S = 1/2$ ) and the excited states ( $S = 3/2$ ) was measured to be 0.315 meV (3.67 K) using inelastic neutron scattering [17]. The  $S = 1/2$  ground states, which are composed of two Kramer doublets, and the first  $S = 3/2$  excited states are depicted in Fig. 1(c). The energy gap of the two Kramer doublets was detected to be  $27 \pm 3 \mu\text{eV}$  [17].

The effective spin Hamiltonian  $V_{15}$  can be described by the  $S = 1/2$  Heisenberg antiferromagnetic model on a triangle [17],

$$H = J_{12}S_1 \cdot S_2 + J_{23}S_2 \cdot S_3 + J_{13}S_1 \cdot S_3 + \mu_B B_0 \sum_{i=1}^3 g_i \cdot S_i. \quad (1)$$

Here  $S_i$  ( $i = 1, 2, 3$ ) denotes the spin operators of the three electron spins localized in the middle triangle, and hyperfine interaction is not included here.  $J_{12} = J_{23} = J_{13} > 0$  here stands for the Heisenberg exchange parameter between electron spins [17]. The  $g_i$ -tensors in the Zeeman term for electron spin are approximately diagonal and isotropic. So the Zeeman splitting of the energy levels does not depend on the relative orientation of the magnetic field to the trigonal axis.

The continuous-wave (cw) and pulsed EPR measurements were performed on an X band (9.7 GHz) EPR spectrometer equipped with the ER4118X-MD5 resonator, Oxford CF935-crystat, and ITC-503 temperature controller from Oxford Instruments Ltd.

The cw EPR spectrum of  $V_{15}$  single crystal was recorded at 100 K and is depicted in Fig. 1(b). It shows a featureless broad first-differential spectrum centered at an effective  $g$ -value of  $g = 1.96$  with about 150 G peak-to-trough. The  $g$  value is slightly less than the free electron value  $g_e = 2.0023$ . This is characteristic for the effect of spin-orbit interaction of the  $3d^1$  electron configuration of  $V^{4+}$  [21]. In the cw EPR spectrum, the hyperfine splitting originating from the magnetic interaction between the unpaired electron and the  $^{51}\text{V}$  nucleus of spin  $I = 7/2$  is not resolved.

For the low temperature pulsed EPR experiments, the  $V_{15}$  solution was prepared in glove box filled with highly-purified nitrogen gas to avoid the oxygen (a known paramagnetic species). The preparation procedure of Ref. [8] was followed.

To record the  $\langle S_z \rangle$  Rabi oscillation, the usual pulse sequence was adopted [22]: a pulse of length  $t$ , a delay time longer than  $5T_2$  and then followed by pulses  $\pi/2-\pi$ . A 10 ns  $\pi$  pulse duration was tried and the oscillation with a strong intensity and period  $T \sim 20$  ns was detected as depicted in Fig. 2 (upper curve). With the same  $B_1$  field, the oscillation period of a standard  $S = 1/2$  sample (P doped in Si) was about 40 ns (using  $t_\pi = 20$  ns). Therefore, the observed upper curve in Fig. 2 was assigned tentatively to be the  $S = 3/2$  of  $V_{15}$ . Then the oscillation of  $S = 1/2$  with period  $T \sim 40$  ns was expected to be detectable using  $t_\pi = 20$  ns, and this was confirmed by the observed new oscillation (lower curve in Fig. 2). We hereby assigned it to  $S = 1/2$  oscillation and accepted the tentative assignment above on  $S = 3/2$  oscillation. Relaxation times were recorded to be  $T_2 = 187.7 \pm 4.4$  ns for  $S = 3/2$  and  $T_2 = 149 \pm 10$  ns for  $S = 1/2$  with echo decay curves shown in the inset of Fig. 2.

The dependence of Rabi oscillations on the driving field strengths was also recorded as shown in Fig. 3(a) for the two low-lying states, and the dependence of Rabi frequencies to the strengths of  $B_1$  field was depicted in Fig. 3(b), which shows clearly the expected proportional relations between the oscillation frequencies and the applied driving field  $B_1$ .

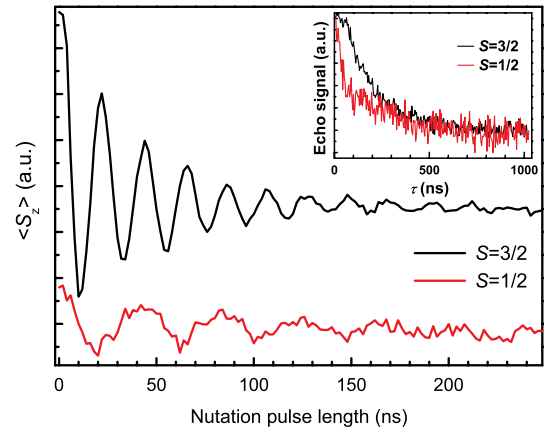


FIG. 2 (color online). The time evolution of the average spin  $\langle S_z \rangle$  after a spin-echo sequence of  $S = 1/2$  states (lower curve), corresponding to the transitions labeled with red arrows in Fig. 1(c), and the  $S = 3/2$  states (upper curve), corresponding to the transitions labeled with black arrows in Fig. 1(c). Inset: the  $T_2$  decay curves for  $S = 3/2$  (upper curve) and  $S = 1/2$  (lower curve) measured with Hahn echo sequences. The experiment parameter settings: The temperature was 2.4 K. For  $S = 1/2$  states,  $B_0$  was set to be 3552 G, microwave power attenuation was 1 dB, pulse duration  $t_\pi = 20$  ns and 20 scans. For  $S = 3/2$  states,  $B_0$  was set to be 3550 G, microwave power attenuation was 1 dB, pulse duration  $t_\pi = 10$  ns and 2 scans.

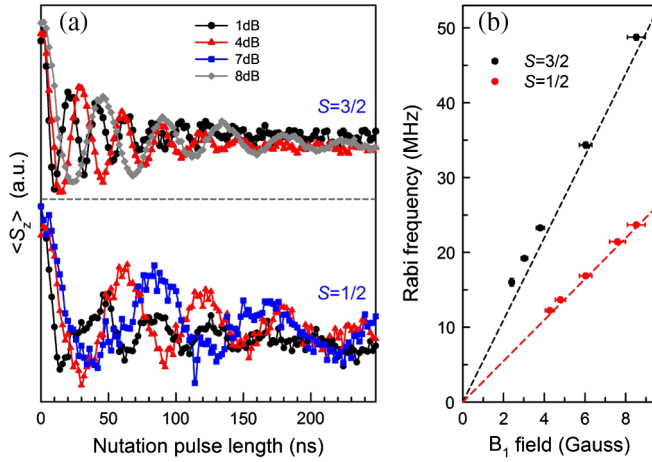


FIG. 3 (color online). (a) Dependence of the Rabi oscillations of both  $S = 3/2$  and  $S = 1/2$  states on the driving field strengths,  $B_1$ . Pulses settings were the same as described in Fig. 2. Temperature was 2.4 K. (b) Corresponding dependence of Rabi frequencies on  $B_1$  field. The  $B_1$  field was calibrated by using the Rabi frequency of a standard  $S = 1/2$  sample (P doped in Si). The dashed lines are the theoretical calculations for  $S = 3/2$  and  $S = 1/2$  as described in the main text.

The following scrutinized measurements and analyses have been done to affirm the assignments of Rabi oscillations in Fig. 2.

Firstly, the wave pattern of the new oscillation is different from the background (cavity) measured with the same experimental parameter settings. As shown in Fig. 4(a), the signal from the background (upper curve) is similar to that reported in [8], as was originally claimed to be the signal of  $S = 1/2$ , where no period oscillation was found. In contrast, the oscillation from the lower curve in Fig. 4(a) (here assigned to be the signal of  $S = 1/2$ ) shows oscillations up to nearly five periods.

Secondly, the detected field-sweep echo-detection (FSED) spectrum of the ground states is different from the background [Fig. 4(b)]. However, the FSED signal does contain the background. Thus the pure EPR absorption of the  $S = 1/2$  states is deconvoluted as the spectrum [the lower curve in Fig. 4(d)] by subtracting the background signal off. With a scrutinized inspection, these background signals shown in Fig. 4(a) and 4(b) have the identical features correspondingly to those being assigned as the  $S = 1/2$  oscillation in [8]. This refutes the previous claimed observation of  $S = 1/2$  Rabi oscillation therein [8] and shows that the new oscillation observed here is genuine. Therefore, the signal observed here is from  $V_{15}$  sample rather than the cavity background.

Thirdly, the Rabi frequency of the new oscillation (23.4 MHz) [can be read directly from the FFT of both oscillations in Fig. 4(c)] is half of that of  $S = 3/2$  (46.9 MHz) measured with the same  $B_1$  field. This agrees with the following theoretical calculation: the Rabi frequency for  $m \rightarrow m + 1$  of the spin  $S$  obeys

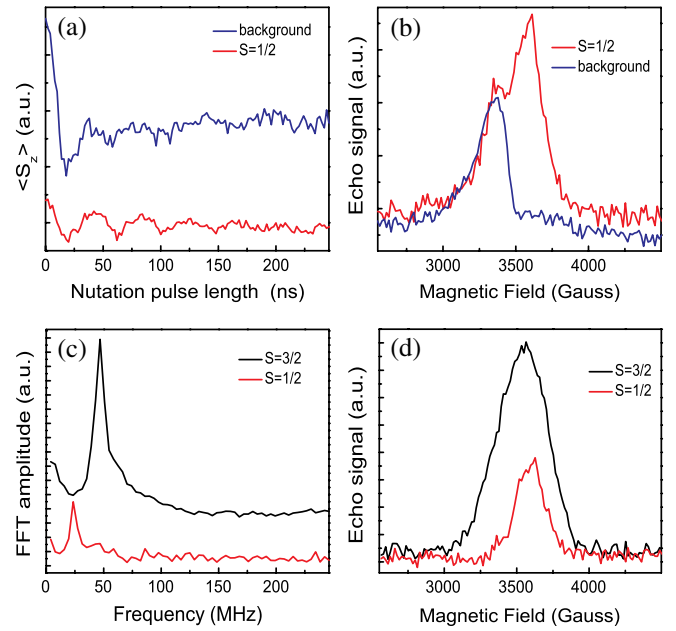


FIG. 4 (color online). (a) The detected Rabi oscillation of  $S = 1/2$  (lower curve) and cavity background (upper curve) observed with the same experimental parameter settings. (b) The FSED of detected  $S = 1/2$  (upper curve) and background (lower curve). (c) The FFT results of  $S = 1/2$  (lower curve) and  $S = 3/2$  (upper curve). The corresponding Rabi frequencies are 23.4 MHz and 46.9 MHz, respectively. (d) The FSED of  $S = 1/2$  (lower curve) and  $S = 3/2$  (upper curve). The signal of  $S = 1/2$  is gained by the detected signal subtract the signal of background (see text).

$\Omega_{S,m} = g\mu_B B_1 \sqrt{S(S+1) - m(m+1)} / \hbar$ , ( $m = -S, \dots, S-1$ ) [22]. With the  $B_1$  field kept unchanged and the almost equal  $g$ -values for the ground and excited states in  $V_{15}$  system, the relationships between Rabi frequencies of  $S = 3/2$  and  $S = 1/2$  are  $\Omega_{3/2,-1/2} = 2\Omega_{1/2,-1/2}$  and  $\Omega_{3/2,-3/2} = \Omega_{3/2,1/2} = \sqrt{3}\Omega_{1/2,-1/2}$ . According to the above formula and the measured  $g$ -value (Fig. 1(b)), the dependence of Rabi frequencies to the  $B_1$  field strengths were predicted to be 5.48 MHz/G for  $S = 3/2$  ( $m = -1/2 \rightarrow m = 1/2$ ) and 2.74 MHz/G for  $S = 1/2$ , which were depicted as dashed lines in Fig. 3(b). Interestingly, the FFT of our measured Rabi oscillation of  $S = 3/2$  state contains only a single peak with a frequency agreeing with the predicted  $m = -1/2$  to  $1/2$  transition. Furthermore, no Rabi oscillation of other frequencies were observed by scanning the  $B_0$  field. This leads us to infer that the quantum oscillations of the  $S = 3/2$  state come predominantly from the  $-1/2$  to  $1/2$  transition. Our experimental results matched well with the theoretical calculation. Obviously, the quantum oscillations and the EPR transitions in the  $S = 1/2$  and  $S = 3/2$  states can be selectively detected by using the appropriate pulse sequence.

In addition, the spectrum pattern of the FSED signal of the ground states [Fig. 4(d)] is similar to that from the  $S = 3/2$  states at 2.4 K. Moreover, the pure EPR

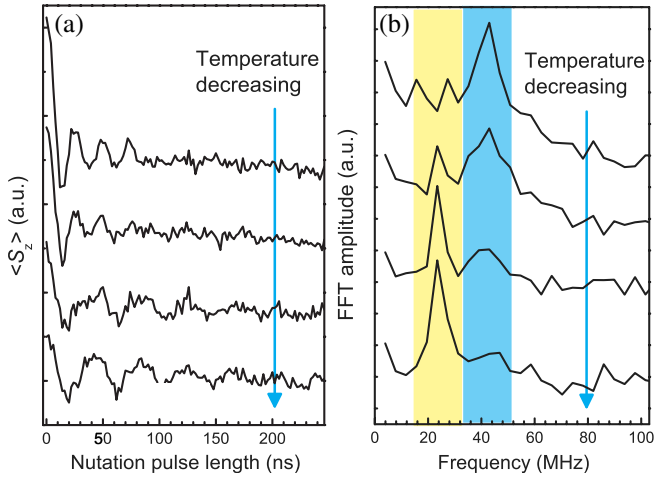


FIG. 5 (color online). (a) Dependence of Rabi oscillation with different temperatures of  $S = 1/2$  states with the same setting described in legend of Fig. 2 but at different temperatures. (b) Corresponding FFT of (a). The main peak of spectra detected at 4.2 K (with the highlighted color of blue around 40 MHz) is originated from  $S = 3/2$ . And the smaller peak shown at the left of the main peak in the spectrum (with the highlighted color of yellow around 20 MHz) is originated from  $S = 1/2$  and it grows larger with lower temperature (see text).

absorption spectrum of the ground states (the resultant subtraction spectrum) shows no obvious deviation in the effective  $g$ -value ( $g = 1.954$ ) compared with the FSED from  $S = 3/2$  ( $g = 1.96$ ).

The pulsed EPR results presented above were measured at the temperature of 2.4 K. The short period (about two hours) stable temperature at 2.4 K used in the measurements shown in Fig. 2 to Fig. 4 was achieved in the following way. At first, liquid helium was pumping into the cryostat for about half an hour with quite a large flow, and then the helium flow was turned off to enable the temperature to drop a little further due to evaporation cooling. This slow temperature decreasing process was monitored by the ITC-503 temperature controller. After about one hour, the temperature finally was stable at 2.4 K, which is the minimal temperature achievable by the present equipment setup. The Rabi oscillations of the  $S = 1/2$  and  $S = 3/2$  states were also chased as temperature decreases from 4.2 K to 2.4 K. The quantum oscillation traces detected by the selective pulse sequence for the  $S = 1/2$  states were shown in Fig. 5(a) together with their FFT transformations in Fig. 5(b).

As mentioned above, the energy gap between the ground states and the first excited states is observed to be  $\sim 3.67$  K. Therefore, the ratio of the population distribution upon the two states may be calculated with Boltzmann distribution combined with the microwave detection operator ( $S_x + iS_y$ ). The calculation shows that the signal intensity of  $S = 3/2$  decreases with lowering temperature, while that of  $S = 1/2$  increases. This is compatible with the trends shown in Fig. 5(a).

The relaxation properties of this complex show its potential application in quantum information processing. At 2.4 K, the  $T_1$  time of  $S = 1/2$  is measured to be about  $12 \mu\text{s}$ , which is three orders of magnitude longer than the nanosecond time scale of quantum control. Compared to the long  $T_1$  time, the  $T_2$  time of  $S = 1/2$  at 2.4 K is only about 149 ns. To expand this short relaxation time, one strategy is to lower the temperature further to reduce the phonon's effect similar to what has been done here in reducing the temperature from 4.2 to 2.4 K. Another probable strategy is to reduce interaction between molecular spins and the surrounding molecular electron spins and the nuclear spins, which is subject to further study.

In conclusion, by realizing a lower temperature combined with adopting a cavity that gives rise to a weaker background than that of the equipment used in Ref. [8], we have successfully detected the signal of Rabi oscillation of the ground states ( $S = 1/2$ ) in trichloromethane solution of single molecular magnet  $[\text{V}_{15}^{\text{VI}}\text{As}_6^{\text{III}}\text{O}_{42}(\text{H}_2\text{O})]^{6-}$  ( $\text{V}_{15}$ ). The FSED of  $S = 1/2$  states was recorded as well, which shows no significant shift of  $g$ -value from that of  $S = 3/2$  states. The detection of Rabi oscillations during the process of lowering the temperature shows that the  $S = 1/2$  signal increases with lowering temperature. As mentioned, the much longer  $T_1$  allows a significant extension of  $T_2$  of this complex [22].

The observing of ground-state quantum oscillation is particularly important in further studies of quantum effect in SMMs. The coherence property of  $\text{V}_{15}$  makes it potentially suitable for qubit implementation, where coherence time can be improved by, for example, using deuterated surfactants and solvent or applying dynamic decoupling approaches [19,20].

This work was supported by the National Natural Science Foundation of China (Grants No. 10834005, 91021005, 21073171, and 31070211), the CAS, and the National Fundamental Research Program.

\*sujihu@ustc.edu.cn

†djf@ustc.edu.cn

- [1] O. Kahn, *Molecular Magnetism* (VCH, New York, 1993).
- [2] D. Gatteschi, A. Caneschi, L. Pardi, and R. Sessoli, *Science* **265**, 1054 (1994).
- [3] M. N. Leuenberger and D. Loss, *Nature (London)* **410**, 789 (2001).
- [4] A. Morello, O. N. Bakharev, H. B. Brom, R. Sessoli, and L. J. de Jongh, *Phys. Rev. Lett.* **93**, 197202 (2004).
- [5] A. Keren, O. Shafir, E. Shimshoni, V. Marvaud, A. Bachschmidt, and J. Long, *Phys. Rev. Lett.* **98**, 257204 (2007).
- [6] A. Ardavan, O. Rival, J. J. L. Morton, S. J. Blundell, A. M. Tyryshkin, G. A. Timco, and R. E. P. Winpenny, *Phys. Rev. Lett.* **98**, 057201 (2007).
- [7] C. Schlegel, J. van Slageren, M. Manoli, E. K. Brechin, and M. Dressel, *Phys. Rev. Lett.* **101**, 147203 (2008).

- [8] S. Bertaina, S. Gambarelli, T. Mitra, B. Tsukerblat, A. Mueller, and B. Barbara, *Nature (London)* **453**, 203 (2008).
- [9] S. Takahashi, J. van Tol, C. C. Beedle, D. N. Hendrickson, L.-C. Brunel, and M. S. Sherwin, *Phys. Rev. Lett.* **102**, 087603 (2009).
- [10] S. Takahashi, I. S. Tupitsyn, J. van Tol, C. C. Beedle, D. N. Hendrickson and P. C. E. Stamp, *Nature (London)* **476**, 76 (2011).
- [11] M. Mannini, F. Pineider, P. Sainctavit, C. Danieli, E. Otero, C. Sciancalepore, A. M. Talarico, M.-A. Arrio, A. Cornia, D. Gatteschi and R. Sessoli, *Nature Mater.* **8**, 194 (2009).
- [12] P. Santini, S. Carretta, F. Troiani, and G. Amoretti, *Phys. Rev. Lett.* **107**, 230502 (2011).
- [13] A. Mueller and J. Doering, *Angew. Chem., Int. Ed. Engl.* **27**, 1721 (1988).
- [14] F. Troiani, A. Ghirri, M. Affronte, S. Carretta, P. Santini, G. Amoretti, S. Piligkos, G. Timco, and R. E. P. Winpenny, *Phys. Rev. Lett.* **94**, 207208 (2005).
- [15] A. Morello, P. C. E. Stamp, and I. S. Tupitsyn, *Phys. Rev. Lett.* **97**, 207206 (2006).
- [16] D. Gatteschi, L. Pardi, A. L. Barra, A. Mueller, and J. Doering, *Nature (London)* **354**, 463 (1991).
- [17] G. Chaboussant, S. T. Ochsenbein, A. Sieber, H. -U. Guedel, H. Mutka, A. Mueller, and B. Barbara, *Europhys. Lett.* **66**, 423 (2004).
- [18] S. Bertaina, S. Gambarelli, T. Mitra, B. Tsukerblat, A. Mueller, and B. Barbara, *Nature (London)* **466**, 1006 (2010).
- [19] J. Du, X. Rong, N. Zhao, Y. Wang, J. Yang, and R. B. Liu, *Nature (London)* **461**, 1265 (2009).
- [20] Y. Wang, X. Rong, P. Feng, W. Xu, B. Chong, J-H Su, J. Gong and J. Du, *Phys. Rev. Lett.* **106**, 040501 (2011).
- [21] A. Abragam and B. Bleaney, *Electron Paramagnetic Resonance of Transition Ions* (Dover, New York, 1986).
- [22] A. Schweiger and G. Jeschke, in *Principles of Pulse Electron Paramagnetic Resonance* (Oxford University, New York, 2001).